RESEARCH ARTICLE

Photovoltaics in the shade: one bypass diode per solar cell revisited

Boudewijn B. Pannebakker, Arjen C. de Waal and Wilfried G.J.H.M. van Sark* iD

Copernicus Institute of Sustainable Development, Utrecht University, Heidelberglaan 2, 3584CS Utrecht, The Netherlands

ABSTRACT

Deployment of residential photovoltaic solar energy systems is strongly increasing, which gives rise to problems such as partial shading and pollution, omnipresent in the built environment. Conventional modules are sensitive to the current mismatches introduced by shadows because of their series architecture of electrical interconnections. This paper presents simulations and experiments showing that a new generation of bypass diodes (BPDs) can be used, up to 1 BPD per cell, to improve the shading tolerance of conventional crystalline modules. We have used cardboard of 0% transmission, and a wire mesh (net) of 38% transmission. The more BPDs are used, the higher the maximum power under shading conditions. Using 20 smart BPDs, or 1 BPD per three cells, leads to an improvement of a factor 3 in power output; for our netting experiments, a factor 1.5 is found. Both performance enhancement and lower diode temperatures lead to increased shade resilience and reliability. © 2017 The Authors. *Progress in Photovoltaics: Research and Applications* published by John Wiley & Sons Ltd.

1. INTRODUCTION

Deployment of photovoltaic (PV) solar energy is rapidly increasing amounting to a global installed capacity of ~230 GW at the end of 2015. About half of this capacity consists of residential rooftop systems, and from a global point of view, this segment is expected to experience stable growth in the coming years [1,2]. Because the cost of PV has decreased fast, retail grid parity in many countries has prompted house owners to invest in PV also at non-ideal locations, that is, locations that are not optimally tilted or oriented, and ones that suffer from (some) shading. This affects PV performance and, in case of shading, introduces mismatches leading to unnecessary and disproportionate losses in energy yield. The disproportionality is attributed to the series architecture of solar cell interconnections of conventional modules, but also to the limited amount of incorporated bypass diodes (BPDs) in modules. Usually a BPD is connected in parallel to strings of 15–24 cells to prevent shaded cells from reaching junction breakdown. This also means that in conventional modules (60/72 cells, with three BPDs), one third of the cells and their power will be bypassed when a BPD is activated. In addition, the activated BPD may heat up significantly as a result of the high currents of today's solar cells and does not prevent hot spots in solar cells. This leads to faster degradation of both diode and solar module in case of partial shading [3,4]. With a further anticipated increase in degree of penetration of PV energy, partial shading, and other mismatch introducing factors (e.g. soiling, manufacturing tolerances, aging, and thermal gradients) therefore require the use of other topologies than presently used.

For PV arrays, solutions to negate mismatches involve different electrical architectures, active or passive reconfiguration mechanisms, changing the number of BPDs or combinations of them together with a variety of control algorithms [5,6]. For residential PV systems, micro-inverters as well as power optimizers per module have demonstrated to increase the resilience to mismatches and therefore the yield [7]. However, to our knowledge, there are only a few commercially available solutions for single PV modules that deal with the mismatches. Nonetheless, solutions at module level are superior because a PV system is in the end dependent on the performance of single modules.

Despite the paucity of existing architectures, several strategies presented in literature could be used to increase the mismatch tolerance of solar modules. One example is the use of "smart" topologies that can utilize a variety of control algorithms to dynamically reconfigure a solar module's internal circuitry (not to be confused with micro-inverters and power optimizers incorporated into a module). These structures are in general based on parallel architectures (total cross-tied or series parallel (SP)) because they are much more resilient to partial shading, as is evident from Kirchoff's current and voltage laws. The switch matrix is a compensation technique that divides a (total cross-tied) matrix of cells into a fixed bank, consisting of several rows of solar cells, and an adaptive bank. Cells in the adaptive bank can form an additional column to compensate for the shaded cells. This has been experimentally demonstrated to increase performance of switch matrices under partial shading conditions for small arrays [8,9]. The application of this technique on module level however involves different requirements for components because module size, energy use, and costs are limiting factors. The conceptual design of an intra-module switch matrix using fully integrated solid-state switches without static power consumption to take into consideration the above-mentioned limitations is shown in [10]. Increased performance under partial shading conditions is claimed however without experimental confirmation. A reconfiguration technique with a somewhat different approach is presented by Wang *et al.* [11], where a PV module is designed with each cell having three integrated switches allowing for either a series or parallel connection. With N being the number of PV cells in the panel, an algorithm can create 1 to N series connected PV-groups, where each PV group consists of a number of parallel connected cells.

Another option is to integrate converters into a module to create sub-module integrated converters (sub-MICs). These can be configured to only process the mismatched part of the power (e.g., they are only switched on when partial shading/a mismatch occurs). Olalla *et al.* [12] show two different ways for sub-MICs to balance and maximize the power output considering one mismatched substring. A similar architecture, called the delta-conversion concept, is presented by Bergveld *et al.* [13]

An approach utilizing the advantage of installing more BPDs in a module is presented by Carr *et al.* [14]. The module consists of metal-wrap-through back-contact multicrystalline silicon (m-Si) solar cells, which are divided into 16 series connected mini-cells, resulting in low-current and high-voltage characteristics. This allows for the use of a smaller BPD (because it has to conduct less current) connected across each cell (i.e., 16 mini-cells), increasing shadow performance significantly, resulting in an almost linear shadow response.

1.1. Smart bypass diodes

A possible disadvantage of many of the above-mentioned techniques is the increase in complexity as they often

require additional sensors and/or switches but also control logic. Furthermore, these techniques require a radically different approach regarding module architecture, and often, some form of power conversion is necessary to obtain the desired current voltage characteristics.

This paper investigates a simple alternative involving the use of a new generation of BPDs to increase mismatch tolerance and module performance under partial shading. Several companies (e.g., Texas instruments, Microsemi, and STMicroelectronics) have recently developed these substitutes to the conventional Schottky BPD called lossless, smart, active, or cool BPDs. They are in fact switching circuits using transistors to mimic diode-like behavior, resulting in a 10-fold lower forward voltage (V_F) (~30 mV) compared with a Schottky diode. As an example, a simplified schematic of the Texas Instruments SM74611 IC [15] is shown in Figure 1. Besides a body diode, an MOSFET, a controller, and FET driver, a charge pump and a capacitor are included. Once a solar cell is shaded, current will flow through the body diode, which creates a potential difference across the anode and cathode. The potential difference charges the capacitor, which in turn powers the IC and turns on the MOSFET. The key to a low V_F is minimizing the charging time (FET off) and keeping a high duty cycle (typical value for duty cycle is between 96% and 99% with FET on for ~240 ms).

The power dissipation and junction temperature, which are problematic for Schottky diodes, are therefore much lower, and this opens up the possibility of incorporating more BDPs into a module than is today's practice. The idea of incorporating more BPDs into a module goes back as far as 1981 [16], while most studies are based on different cell architectures using integral BPDs [16–18]. Lefevre *et al.* [19] present a comprehensive study where the performance of different SP configurations in combination with a varying number of bypass and blocking diodes is simulated. Three of these SP configurations in combination with two shadow patterns (tree and pole) were experimentally tested.

The aim of our paper is to determine if the above-mentioned smart BPDs can be used to increase mismatch tolerance of a series topology with conventional solar cells. All the proposed topologies will be tested both experimentally in a dedicated module and through simulations using the Python programming language.

This paper is further organized as follows. We first review the effect of partial shading on PV performance and the role of BPDs in Section 2. We then present our experimental and simulation methodology in Section 3. Results are shown and discussed in Section 4, which is followed by Section 5 on the potential of the use of BPDs for shade-resilient modules. After a thorough discussion of the result in Section 6, Section 7 concludes our paper and provides recommendations for further research.

2. PARTIAL SHADING

As the basic operation of PV cells and modules, shaded and unshaded, is already well known and described, we
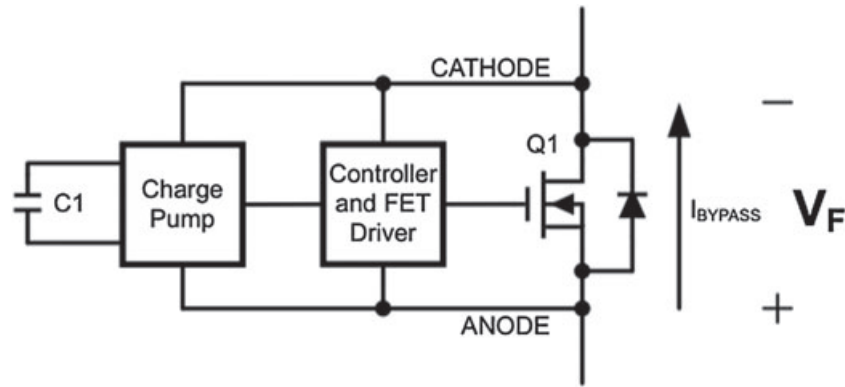
Figure 1. Diagram of the Texas Instruments SM74611 IC [15].

refer to textbook literature, for example, [20], which provides an excellent overview regarding the interpretation of the performance of PV cells through the IV curve and its most important parameters, that is, open circuit voltage (V_{OC}), short circuit current (I_{SC}), maximum power (P_{MP}), series resistance (R_S), and shunt resistance (R_{SH}). The effect of partial shading and the effect that BPDs have on the shape of IV curves is treated in literature [21–23], while details on performance ratio are reviewed by Reich *et al.* [24].

2.1. The role of BPDs

Shading a solar cell mainly reduces the current of a solar cell, as its current is directly proportional to irradiance. Once shaded, a cell is forced to operate in reverse bias by the other cells in the string to be able to conduct their higher current levels. It thus acts as a load and dissipates power, resulting in localized heating. In the worst case, the cell can be irreversibly damaged, which is generally referred to as a hot spot-induced malfunction. The maximum reverse voltage and therefore the maximum power dissipation in a single shaded cell are determined by the number of cells in the string, their V_{OC} (typically ~0.6 V) and the forward voltage (V_F) of the BPD [25]:

$$|V_{\text{rev}}|_{\max} \leq \left(\Sigma_{i=1}^{\text{cells/string}-1} V_{cell,i} + V_F \right) \quad (1)$$

Strings are therefore generally not larger than 24 cells because including more would increase the chance of reaching junction breakdown voltage, which is generally in the order of -15 V for crystalline silicon cells. Note that a BPD does not prevent a cell from dissipating power because it has to operate in reverse bias in order to overcome the positive bias in the string and activate the BPD [25]. Once a BPD is activated, it provides an alternative route for the surplus current of the other strings as shown in Figure 2. This does however mean that one shaded cell can reduce the power of a conventional module by one third (60/72 cells, three BPDs). In the absence of BPDs, the power loss could be even greater.

From a shade resilience point of view, it would be better to incorporate more BPDs because smaller strings will be bypassed in the case of partial shading [22]. However, today's 6-in solar cells reach currents up to 9 A. For conventional Schottky BPDs, this results in an increase of V_F (up to ~0.45 V instead of ~0.35 V) and a power dissipation of ~4 W. Consequently, junction temperatures reaching 150 °C are not uncommon [3,26]. Manufacturers therefore install heat sinks in junction boxes and limit the amount of BPDs as increasing their number also increases the chance of one of them failing. Information on failing rates of BPDs in the field is unfortunately not widely available, only one non-representative study on defective BPDs is available, which shows a large number of malfunctions [27]. The previous one advocates the use of different, more shading-tolerant, module architectures.

2.2. Impact

The loss of power due to mismatches depends on several variables including cell interconnections, PV-system configuration (i.e., parallel vs. series), inverter type (central, micro, or power optimizer), and shadow pattern, which makes quantification difficult. Nonetheless, since the early 1990s, several large-scale performance studies provide estimates about performance loss including shading losses [28–31]. However, the methods to determine the loss differ, which is also reflected in the range of the estimations of shading loss (~2–10%). The main problem is that irradiance data with a high spatial and temporal resolution is required to accurately determine the shading loss [22]. A recent PV performance study among 5000 investigated residential PV systems across the Netherlands shows that about 10% of these is affected by some form of shading, resulting in a loss of ~5% [32]. Participants to this study could comment if their systems were hindered by shade, although this was not obligatory. A share of 10% is therefore considered a conservative estimate. In reality, the majority of residential systems probably deals with shading to some extent [7,28], which is also reflected in the distribution of the performance ratios of systems for which no shade was reported. More
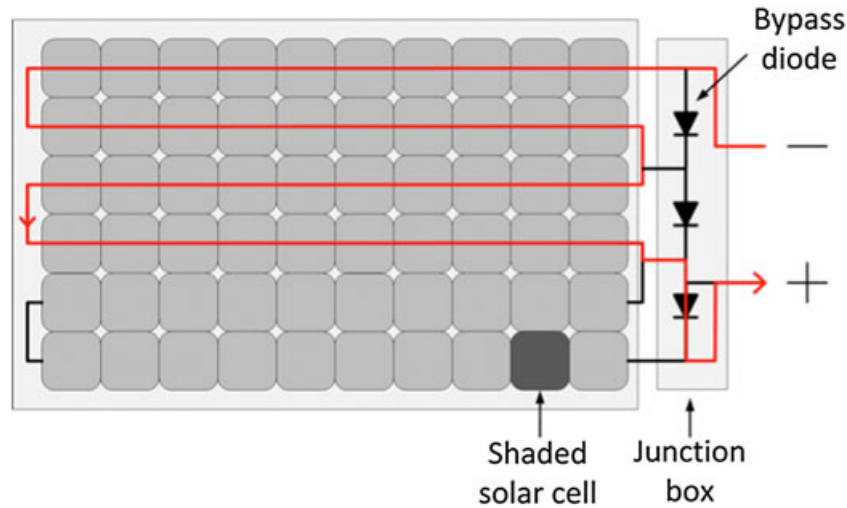
Figure 2. PV module with one shaded solar cell, which results in the bypass of one string of 20 solar cells. [Colour figure can be viewed at wileyonlinelibrary.com]

research on this topic is required to gain insight into the true extent of the impact.

Furthermore, part of the power lost due to shading is attributed to the reduction in irradiance while the remaining power loss is attributed to the inability of modules to deal with mismatches. The shade impact factor (*SIF*) can be used to estimate the recoverable amount of power [33]:

$$SIF = \left[1 - \frac{P_{\text{shade}}}{P_{\text{sys}}}\right] \frac{A_{\text{sys}}}{A_{\text{shade}}} \qquad (2)$$

in which P_{shade} is the power produced under shaded conditions, P_{sys} is the nominal system power, A_{sys} is the system area, and A_{shade} is the shaded area. Shading half a cell can lead to an *SIF* of 40 (for 1 BPD per 20 cells), which means that the reduction in power is 40 times greater than the shaded area would suggest. An *SIF* of 2 has been adopted by the California Energy Commission as a constant penalty factor for expected performance of shaded solar modules [34]. In other words, we believe that at least half of the lost energy could be recovered. This is however considered a very conservative estimate [33].

3. METHODOLOGY

3.1. Experiment design

We investigate a simple solution for conventional modules to increase their mismatch tolerance to shading. Only series architecture of solar cell interconnections is therefore considered because parallel structures would need additional power conversion steps to connect to conventional inverters/system components (i.e., six parallel strings would deliver ~50 A). Overlapping

structures for the diodes are not considered because they do not seem to benefit overall performance [35,36]. The BPDs are connected in parallel across 1, 3, 5, 10, and 20 solar cells, which results in the use of 60, 20, 12, 6, and 3 BPDs, respectively. They are installed across vertical strings of solar cells in a portrait-oriented module, for example, for the six BPD configuration, a BPD is connected across cell 1–10, 11–20, 21–30, 41–50, and 51–60, as indicated in Figure 3(a). For the 20 BPD configuration, the BPDs are connected across cells 1–3, 4–6, 7–9, and others. The four shadow patterns (Figure 4) that will be used are row, column, random, and corner. These represent common shadowing shapes that appear in the built environment, such as poles, chimneys, dormer windows, and row-to-row shading of modules. Two materials were used for the shadow patterns: cardboard with 0% transmission and a wire mesh (net) with ~38% transmission. Together, this results in a total of 40 different experiments: five BPD configurations times four different shadow patterns times two shadow materials.

3.2. Experimental setup

A dedicated reconfigurable module specifically made for testing shadow tolerance was constructed for this project (Figure 3(b)). The module consists of 60 m-Si solar cells (156×156 mm^2) manufactured by Solland Solar belonging to a power class of 3.65 W; module rated capacity thus was 219 Wp. All cell terminals are located externally, at the back of the module. The module has a black backsheet, and the rear of the module was left open so that cell interconnections could be made externally. To achieve this, a switchboard was constructed in a 5-mm thick Plexiglas plate that was later attached to the back of the module. The switchboard consists of 120 female plugs (both polarities for each of the 60 cells). Copper wires of ~70 cm (1-mm diameter) were soldered to the strips of
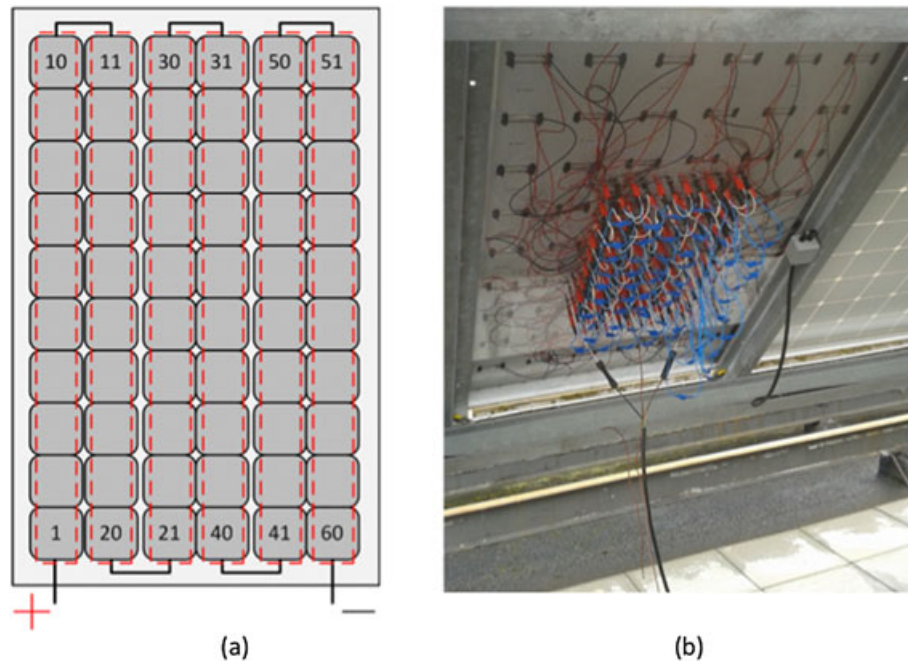
Figure 3. (a) Schematic back side of the module with numbered solar cells. The red dashed rectangles represent six BPDs connected across strings of 10 cells. (b) Photograph of the dedicated solar module. The blue wires represent the BPDs while the white wires facilitate the electrical connections. [Colour figure can be viewed at wileyonlinelibrary.com]
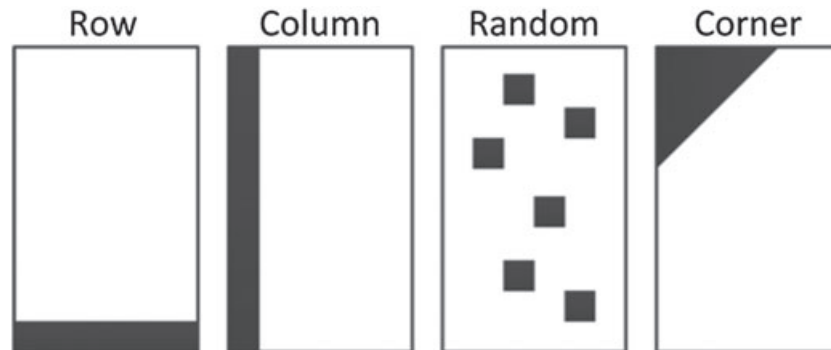
Figure 4. Shadow patterns that were applied.

the solar cells and connected to the female plugs in the Plexiglas plate. In this way, any possible electrical configuration can be realized; however, at the expense of adding substantial series resistance R to the module circuit ($R = \frac{\rho*l}{A} = \frac{1.68e^{-8}\Omega m*1.4m}{\pi*(5e^{-4}m)^2} = 0.029\Omega$, with ρ specific resistivity of copper, l length of the wire and A its cross-section). The male plugs, connecting the solar cells include a second opening for the BPDs. The smart BPDs used in this project are manufactured by Texas Instruments, type SM74611 [15]. Their power dissipation is in the range of 0.2–0.4 W while Schottky diodes dissipate ~4 W, resulting in a significantly lower junction temperature.

The measurements were performed outdoors at the Utrecht Photovoltaic Outdoor Test facility [37] on the Utrecht University Campus, the Netherlands. An MS-802 pyranometer (accuracy ±2%) developed by EKO instruments measures global plane-of-array irradiance (module tilt is 37°). Because the pyranometer and module in practice were located about 15 m apart, the irradiance can differ. However, measurements were conducted on clear-sky days. The temperature is measured by a thermocouple attached with thermal paste to cell 36 (mid module, Figure 3(a)). Both the module and pyranometer were placed at a 37° angle facing south. An IV tracer developed by EKO instruments, type MP-160 (accuracy ±~0.5%), was used for measuring the IV curves of both the module and the individual cells. Acquiring one IV curve required ~3 s. The IV data (I_{SC}, V_{OC}) of the individual cells will be used in the simulation model.

3.3. Simulation model

The PV performance simulation model was built in Python using functions from the PVLIB toolbox provided by the PV performance modeling collaborative [38]. IV curves were generated with the one-diode model, following [39]

$$I = I_{PH} - I_S \left[\exp\left(\frac{V + IR_S}{n\,V_T}\right) - 1 \right] - \frac{V + IR_S}{R_{SH}} \quad (3)$$

where I_{PH} is the photocurrent; I_S is the diode saturation current; R_S and R_{SH} are the series and shunt resistances, respectively; n is the diode quality factor, and V_T is the thermal voltage. These parameters were adjusted to environmental conditions using equations presented by De Soto *et al.* [40].

the IV curves of the 60 cells were simulated under outdoor conditions with varying cell temperature (54–56.8 °C) and irradiance (632–744 W/m^2), corresponding to the conditions at which the experiments were performed. The simulated IV curves were fitted to the experimental IV curves using nonlinear least square fitting with the function LMfit in Python. A set of individual parameters was created for each of the 60 cells (Table I). Note that I_{PH} was set equal to the measured I_{SC} of each individual cell. The optimized mean value for R_S corresponds to the resistance due including the internal 1.4-m wiring (Section 3.2). Diode losses were incorporated by applying a voltage drop of 40 mV per activated diode and a leakage current of 0.5 µA for inactivated BPDs. For determining the true potential (Section 5), a conventional (low) value for R_S is considered, and resistance losses due to the extra wires and plugs are not incorporated. Diode losses however are incorporated.

4. RESULTS AND DISCUSSION

4.1. Unshaded IV curve

A measured IV curve of the module containing three BPDs receiving uniform irradiance is shown in Figure 5. The shape of the IV curve reveals two important characteristics:

(1) Near I_{SC}, that is, from 0–15 V, there is a clear cascade visible. This can be explained by either a power difference in the cells or a difference of resistance between a cell's wires and electrical components. The cascade shows the function of the three BPDs that were incorporated for these measurements.

(2) For voltages >15 V, a clear resistive behavior is observed. This is attributed to the high series resistance caused by the many wires, plugs, and connectors incorporated into the experimental module. The high R_S limits the power output significantly, but does not change the shadow response of the module.

Table I. Parameters from fitting the 60 individual cells at measurement conditions (temperature range 54–56.8 °C and irradiance range 632–744 W/m^2).

	Fitting results		
	Mean	Lower	Upper
R_S (Ω)	0.0399	0.0382	0.0447
R_{SH} (Ω)	13.34	5.02	16.67
n	1.20	1.13	1.25
I_S (A)	9.26×10^{-7}	3.87×10^{-7}	1.00×10^{-6}
I_{PH} (A)	6.047	5.442	6.547
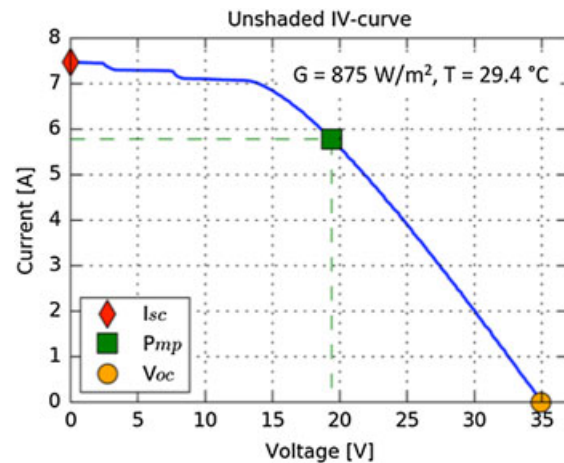
Figure 5. Unshaded IV curve measured at irradiance of 875 W/m^2 and ambient temperature of 29.4 °C. [Colour figure can be viewed at wileyonlinelibrary.com]
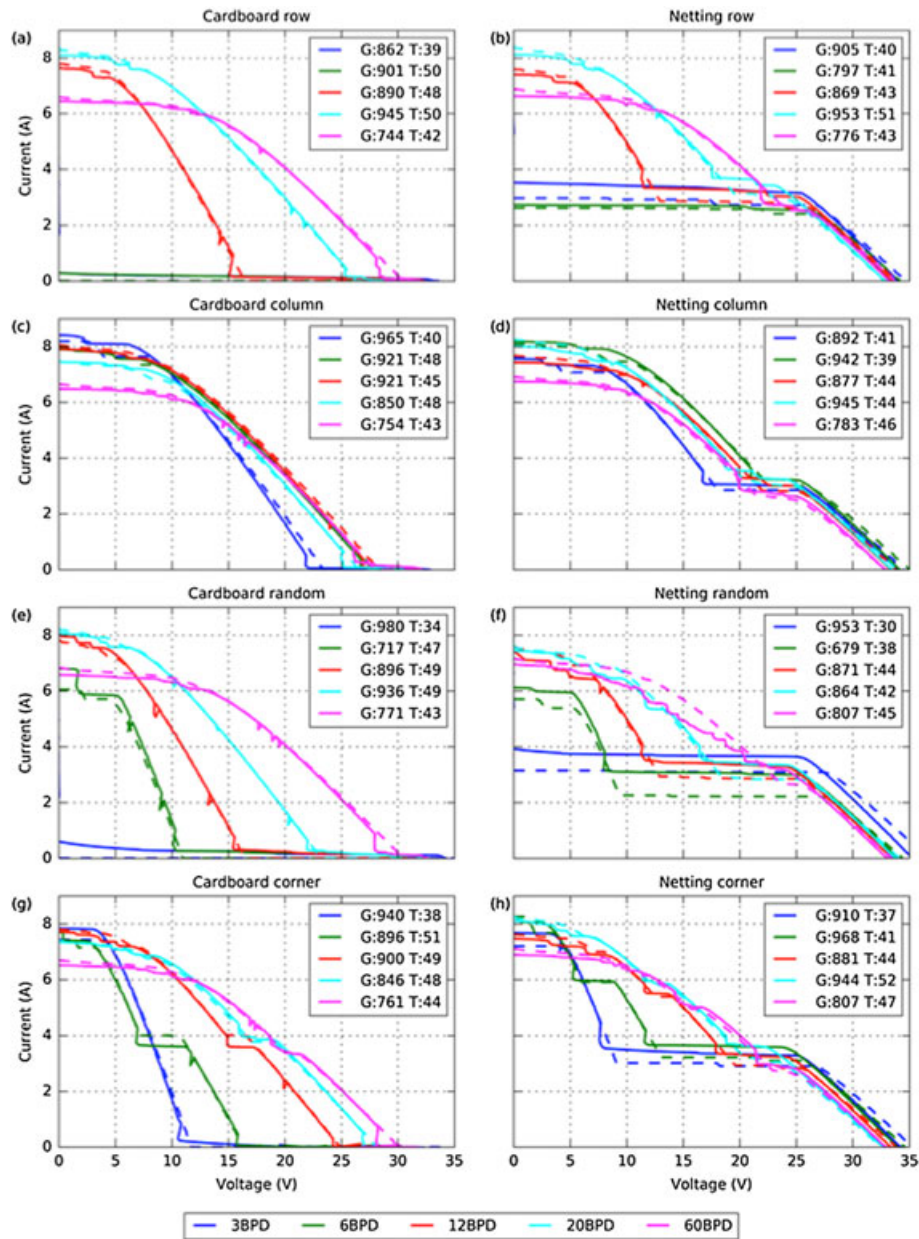
4.2. Experiment

Both the measured (solid lines) and simulated (dashed lines) IV curves are shown in Figure 6. Each subplot shows the IV curves of the five different BPD configurations for a specific shadow pattern and material. Because the experiments were conducted outdoors, ambient temperature (T) (30.0–51.8 °C) and irradiance (G) (680–980 W/m^2) varied uncontrollably. A higher value for I_{SC} and/or V_{OC} does therefore not necessarily imply better performance of the configuration. It is however still useful to examine the IV curves because their shapes provide valuable information about the performance of the different configurations in response to the shading experiments.

4.2.1. Measured IV curves.

The main findings/observations regarding the measured IV curves are

- The BPDs function well because they are activated by the shadow patterns (e.g., Figure 6(h)).
- The shadow materials function as expected: cardboard completely blocks all irradiation while the

Figure 6. Measured (solid lines) and simulated (dashed lines) IV curves of the experiment with cardboard shading patterns (a, c, e, and g) on the left and netting (wire mesh) shading patterns (b, d, f, and h) on the right. The shading patterns are from top to bottom: row, column, random, and corner. The number of bypass diodes was changed during the experiments, and the color-coded solid (and dashed) lines uniquely link to the number of bypass diodes used. In every graph, the sequence of colors (top to bottom in one graph) is 3, 6, 12, 20, and 60 BPDs, with colors blue, green, red, light blue, and purple, respectively. As during the outdoor experiments both irradiance (G in W/m^2) and temperature (T in °C) varied, their values have been added as well in the legends of the subplots. [Colour figure can be viewed at wileyonlinelibrary.com]

wire mesh blocks only a part, which is evident from the distinctive knees in many of the IV curves (Figure 6(b),(d),(f),(h))

- The orientation of the shadow pattern (i.e., horizontal or vertical) greatly affects the performance (cf. Figure 6(a),(b) and Figure 6(c),(d)). This is explained by the vertical orientation of the BPDs. As a result,

horizontally orientated shadow patterns bypass more strings.

- The knees in the curves for cardboard corner are explained by the fact that 50% of four cells is completely shaded (Figure 6(g)).
- The potential drop of the smart BPDs is small compared with conventional Schottky diodes,

demonstrated by column shade where 10 BPDs are active in the 60 BPD configuration compared with one active BPD in the six BPD configurations (Figure 6(c),(d)). A large difference in V_{OC} is not observed, while in both cases 10 cells are bypassed (e.g., with Schottky diodes there would be an additional drop of ~4–6 V for the 60 BPD configuration).[1]

- For some cardboard shadow patterns (Figure 6(a),(e), (g)) the current does not decrease to zero while it should because cardboard is supposed to completely block all irradiance. Apparently some irradiance did reach the cells during the experiments, because of "leaking" at the edges.
- Several of the curves show small dips (Figure 6(a), (e),(g)). A possible explanation for this behavior is the internal circuitry of the smart BPDs as explained in the introduction. After activation, current flows through a body diode, which allows a capacitor to be charged, which in turn powers the MOSFET. The dips that are visible in the IV curves could be related to this switching and charging behavior.
- The curve for the 60 BPDs netting random configuration (Figure 6(f)) shows many dips and deviates from the expected shape. A possible explanation could be drops in irradiance during the measurement.

Overall, we conclude that the different configurations and shadow patterns behave as expected. The main functioning of the smart BPDs is proven because they bypass when expected while having a much lower V_F.

4.2.2. Simulated curves.

In general, there is good agreement between the measured (solid line in Figure 6) and simulated (dashed line in Figure 6) curves as the simulation model bypasses the strings that are shaded and follows the general shape of the curves. There are however also some discrepancies. There seems to be an overestimation of simulated current values in the knees of the cardboard IV curves, and an underestimation for the netting material. The deviations are especially large for the three BPD netting row configuration (Figure 6(b)) and for the three and six BPD netting random configurations (Figure 6(f)). In addition, the I_{SC} value for the measured curve of the 6 BPD cardboard random configuration is considerably higher than the simulated I_{SC} value. The average mean average error (MAE) for all full I–V curves is 4.04%. For most of the situations, MAE < 5%, with a maximum of 14.7% in one case (six BPD cardboard random), which can be explained by an experimental issue (the cardboard did

most probably not fully cover the module). For P_{MP}, the average MAE was 2.15%. For most of the situations, MAE < 4%, with a maximum of 7.8% in one case (6 BPD cardboard random).

Both the discrepancies between the measured and simulated curves and the unexpected spikes and voltage drops of the measured curves are likely explained by the nature of the experiment:

- The experiments were conducted outdoors in a limited timeframe. Because there was about 15 m distance between the pyranometer and solar module, irradiance values may have differed between the two locations. Furthermore, irradiance may have also changed during the experiment.
- The netting material seems to transmit more irradiation. Repeated use of the flexible material may have resulted in a smaller surface area, which leaves the edges of the solar cells open for full irradiance. For example, a 2-mm gap between the cell edge and shadow material edge represents ~5% of the total cell area. For the netting material, this would result in an increased average transmission for the cell of ~41% instead of 38%.
- Experiments were executed in rapid succession, that is, without temperature stabilization.
- The wires that facilitate the electrical interconnections, the smart BPDs, and accompanying wires and plugs were connected randomly for the conducted experiments. In other words, different wires and BPDs were connected to different cells for the experiments. During handling, some connections may have deteriorated, resulting in a possible increase in resistance.
- Discrepancies between the expected and observed IV curves may also be explained by the effect of shunt resistance on diode activation, as pointed out by Lim et al. [41]. Solar cells are not tested on shunt resistance while it affects diode activation greatly.

The simulation model works adequately well, considering the many different experiments, the varying environmental conditions, the fact that 60 curves were generated for each experiment (individually fitted to the experimental data of each cell), the fact that there is a power difference between the cells and taking into account the high series resistance due to the incorporated electrical components to conduct the experiment.

4.2.3. Summary.

Notwithstanding its limitations, the experiments do serve as a proof of principle: the BPDs function well (i.e., are activated and have a lower V_F) under a variety of irradiance conditions and different topologies. Furthermore, the simulation model in most cases follows the shape of the curves and bypasses strings when they are shaded. The discrepancies are mainly attributed to the nature of the experiment.

---

[1]The temperature of the 60 BPD configuration is 5 °C lower, which has a positive effect on V_{OC}. However, looking at the linear relationship for V_{OC} and temperature presented in Section 4.1, this would amount to a difference of ~0.5 V.

It is clear that the module has a high series resistance because of the many plugs, wires and interconnectors, which was to be expected. Furthermore, there is a small power difference between the cells, which could be due to the solar cells themselves, because of a difference in resistance of the wires and electrical components, or a combination of the two.

The high series resistance combined with the changing environmental conditions makes it difficult to compare the performance of the different topologies and thus the true potential of diode incorporation. Therefore, in the next section, we will explore this potential by simulating the same set of experiments but with a normal value for R_S and without a power difference between the cells.

5. TRUE POTENTIAL: SIMULATED PERFORMANCE AT STANDARD TEST CONDITIONS (STC)

5.1. Unshaded module

The solar cell and module parameters used in the simulation to determine the true potential of employing smart BPDs in the PV module are listed in Table II. As a reference, the parameters of the datasheet of the m-Si solar cell (156×156 mm^2) manufactured by Solland Solar belonging to a power class of 3.65 W were used. R_{SH} and n are the average optimized values from Table I while R_S and I_S were optimized to match the module performance values.

The characteristics of a panel including 60 of these cells and the simulation model performance are summarized in Table III. There is less than half a per cent difference between the datasheet values and simulation model values.

5.2. Shading simulation results

The P_{MP} for each configuration normalized to the unshaded P_{MP} is shown in Figure 7. The average performance of the four shadow patterns for each BPD configuration is indicated by the horizontal pink bars. The 3 BPD configurations can be seen as the conventional reference cases.

For the cardboard shadow patterns, there is, besides some exceptions, an increase in performance with an increase of incorporated BPDs. There are three configurations, row shade 3 and 6 BPDs and random shade

3 BPDs, where the panel produces 0 W. This is because, in these configurations, the shadow patterns bypass all strings/cells in the module. For column shade, the 6 and 12 BPD configurations outperform those of the 20 and 60 BPD configurations, which can be explained by the fact that less BPDs are activated to bypass the shaded cells/strings. The 20 BPD configuration performs about 3% lesser than the 60 BPD configuration because of the string topology, that is, 12 cells instead of 10 are bypassed.

For the netting shadow patterns, there is also an increase in performance with an increase of incorporated BPDs. The performance of the three and six BPD configurations for row, column, and random shadow patterns is nearly the same. The shape of the IV curves, however, is different, as is evident in Figure 8 in which IV curves for the netting shadow patterns of the six BPD configurations are shown. The maximum power points of the row, random, and corner shadow patterns are all located at high-voltage levels and a current level of ~3 A (dictated by the ~38% transmission of the netting material). However, the shape of the curve above 3 A is different.

The performance values for all the shadow patterns for the 20 and 60 BPD configurations are the same for cardboard and netting, as is clear from Figure 7. This has a similar reason as explained in Figure 8; the shapes of the actual IV curves differ, but the values for V_{MP} and I_{MP} are similar, but now at a higher current and slightly lower voltage.

On the basis of the graphical representation of results previously, a metric is proposed that allows to quantify the benefits of using more BPDs than is commonly used today. We define the figure of merit F_{BPD} as the ratio of P_{MP} and unshaded P_{MP}, relative to the same ratio for the case of 3 BPDs, as follows:

$$F_{\text{BPD}} = \frac{\frac{P_{MP}(i)}{P_{MP,\text{unshaded}}(i)}}{\frac{P_{MP}(3)}{P_{MP,\text{unshaded}}(3)}} \quad (4)$$

with i the number of diodes (3, 6, 12, 20, or 60). The results are shown in Figure 9, in which we have summarized the results for cardboard and netting (the pink horizontal bars in Figure 7). The error bars reflect the standard deviation of the mean, which is large for the cardboard cases as the P_{MP} at row shading are zero. It can be seen that using one diode per cell leads to 3.43

**Table II.** Solar cell and module parameters with low R_S.

	Cell	Module (60 cells)
R_S (Ω)	2.7×10^{-3}	0.163
R_{SH} (Ω)	13.3	800.4
n	1.2	72
I_S (A)	2.807×10^{-8}	2.807×10^{-8}
I_{PH} (A)	7.93	7.93

**Table III.** Cell and module performance at STC conditions.

	Datasheet H-cell	Model	Difference (%)
I_{SC} (A)	7.93	7.93	—
V_{OC} (V)	35.82	35.88	0.17
I_{MP} (A)	7.44	7.41	−0.40
V_{MP} (V)	29.58	29.52	−0.20
P_{MP} (W)	219	218.7	−0.14
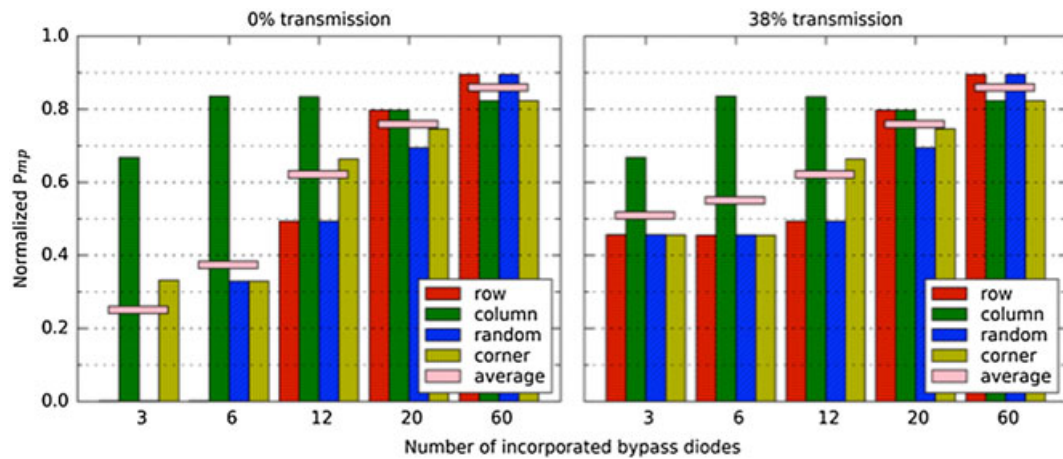
Figure 7. Results of simulations of P_{MP} normalized to the unshaded P_{MP} for cardboard (left) and netting (right). The x-axis shows the number of incorporated bypass diodes. The average performance of the four shadow patterns for each BPD configuration is indicated by the horizontal pink bars. [Colour figure can be viewed at wileyonlinelibrary.com]
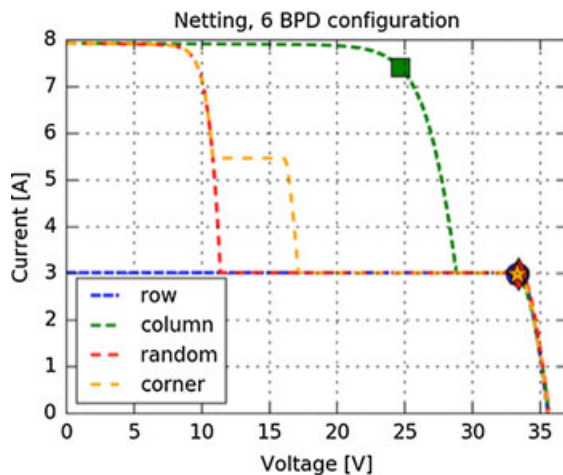
Figure 8. Simulated IV curves of the netting shadow patterns for the six BPD configurations. The markers indicate P_{MP}. [Colour figure can be viewed at wileyonlinelibrary.com]
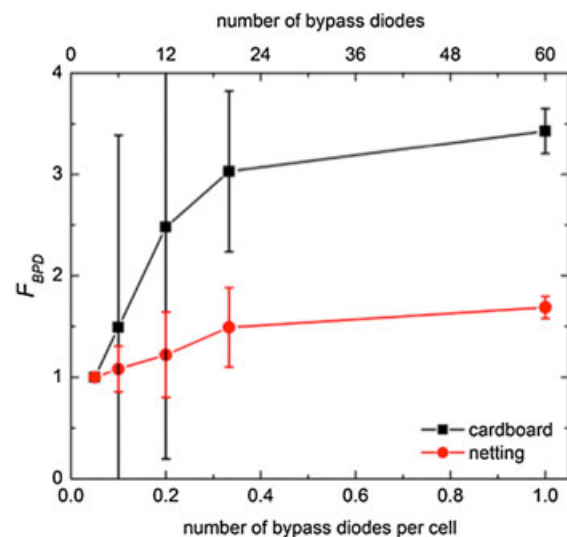
Figure 9. Figure of merit F_{BPD}: ratio of P_{MP} and unshaded P_{MP} for the number of BPDs per cell relative to the standard case of three BPDs per module of 60 cells. Error bars are standard deviations of the mean of the four types of shading for cardboard and netting. [Colour figure can be viewed at wileyonlinelibrary.com]

times more power compared with the standard case should be case of three diodes per 60 cells in case of the cardboard shading experiments. For the netting experiments, the use of one diode per cell leads to 1.69 times more power. Adding more than 20 diodes per module leads to modest improvements only.

Although the normalized performance is useful in analyzing the performance of the configurations, it does not take into account the shaded area of the different patterns. We have therefore plotted the shade impact factors (see Equation(2)) in Figure 10 to provide an indication of the linearity of the shadow response and thus how much power is recoverable/wasted. For example, an *SIF* of 10 indicates that the power loss is 10 times greater than the loss in irradiance (e.g., row shade involves six shaded cells, while the output for the three and six BPD

configurations is 0 W; thus, the loss of 10 × 6 cells). Clearly, the 60 BPD configuration nearly has a complete linear response to the shadow patterns.

It is further found that smaller strings increase the shadow resilience of panels drastically (Figures 8–10). However, they do not provide information about I_{MP} and V_{MP}, which are important for determining if a panel can contribute to power generation. When I_{MP} is the same or higher than the string I_{MP}, the BPDs remain inactivated and the panel contributes to power generation. When I_{MP} is lower, the BPDs will be activated to conduct the higher
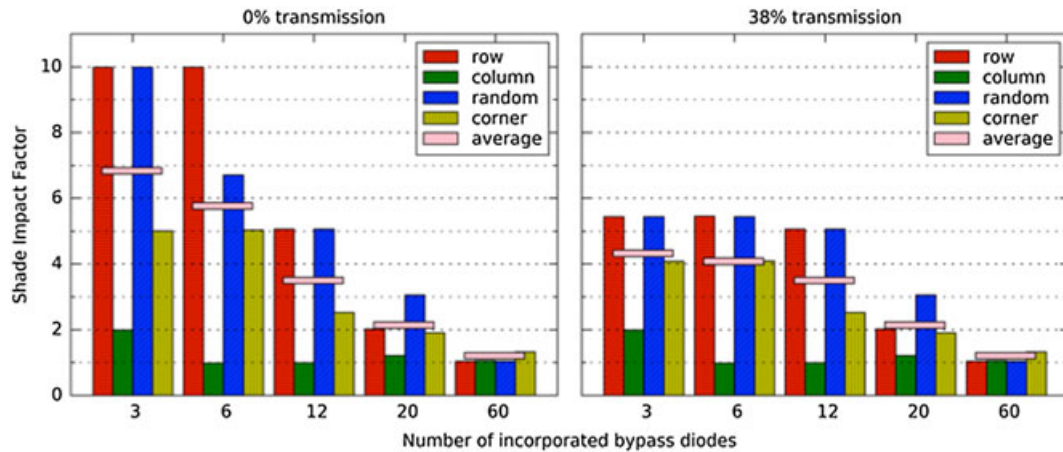
Figure 10. Shade impact factor for cardboard on the left and netting on the right. [Colour figure can be viewed at wileyonlinelibrary.com]

string current and the power of the shaded module is lost. An alternative way of showing shading effects is presented in Figure 11, which includes I_{MP} and V_{MP} values. The color indicates normalized P_{MP} for all subplots, while the size of the circles is proportional to I_{MP} for the top two subplots and proportional to V_{MP} for the bottom subplots. It is clear that I_{MP} has the same value for all shadow patterns and BPD configurations once 12 or more BPDs are incorporated. This means that these configurations would still contribute to power generation in a PV system containing a number of unshaded modules. For V_{MP}, large differences are observed for the 3 and 6 BPD configurations, with relatively high values for the netting material and zero-to-low values for cardboard. Excluding

these configurations, there is a general increase in V_{MP} for an increase in incorporated BPDs.

6. DISCUSSION

We have shown and re-confirmed in this work that the more BPDs are incorporated in a PV module the lower the effect of shading is on the power output. In other words, more BPDs lead to shade-resilient modules and therefore less economic loss to shading.

However, cost of smart BPDs is considered to be a barrier for market introduction. The new BPDs discussed in this paper can be purchased presently at about $1.50
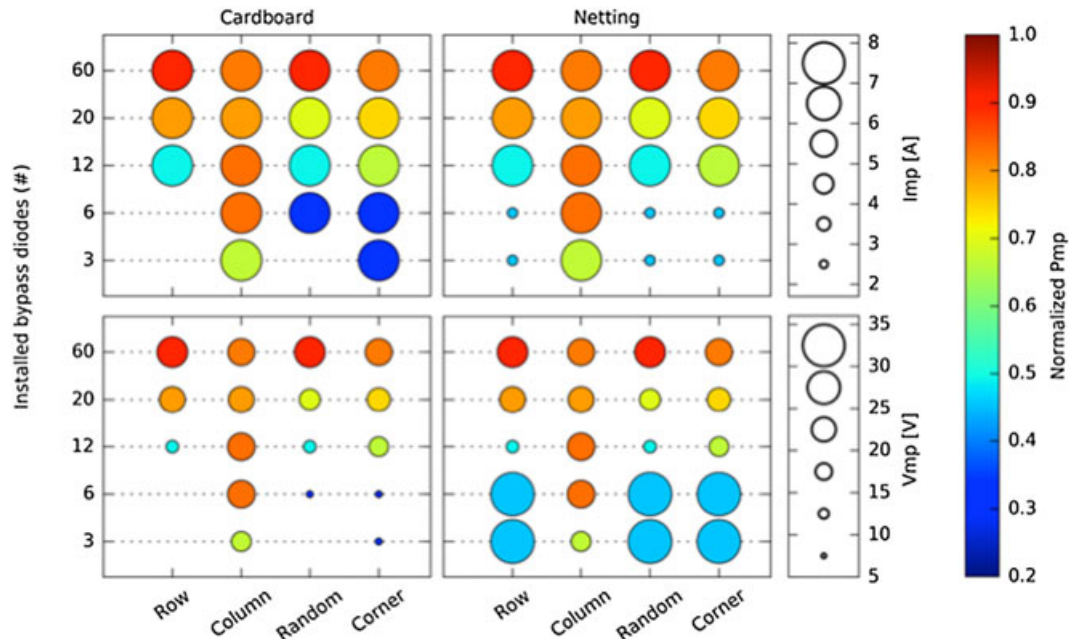

Figure 11. Normalized P_{MP} (color) for cardboard (left) and netting (right). The size of the circles is proportional to I_{MP} for the top two figures and V_{MP} for the bottom two figures. [Colour figure can be viewed at wileyonlinelibrary.com]

per piece at quantities of 1000, while present cost of Schottky diodes is around $0.16 per piece at very high quantities. With average module rated capacity of 270 Wp and three diodes per module, this amounts to $0.48 per module, or diode cost of 0.0018$/Wp.

Integrating 20 new BPDs, perhaps in the backplane of the module, will lead to higher module cost, that is, adding ~0.11$/Wp to the present module cost of ~0.40$/Wp. However, modules with these diodes are much more shade resilient. Assuming that a PV system has a yield of 1000 kWh/kWp, and a feed-in tariff of 0.10$/kWh is in force, the benefit of overcoming the average 10% loss in performance due to shading would amount to a benefit of 10$/kWp annually. With present BPD cost of $1.50, this would therefore not be feasible. Thus, if BPD cost could be lowered to $0.15 per piece, the payback time of this additional cost would be about 1 year. Given that economies of scale lead to much lower BPD cost, this 10-fold lowering of cost can be seen as realistic, which is corroborated by the fact that a 500-MWp PV factory needs over five million BPDs (three per module) today.

Besides a potential economic benefit due to performance improvement, smart BPDs well have lower temperatures when activated. Using datasheet information, at a current of 8 A and a worse case of 125 °C, about 0.5 W is dissipated in a smart BPD compared with some 4 W for a Schottky diode, which is due to the different operating principle. Typically, junction temperatures in smart BPDs are 50–80 °C lower in temperature than Schottky diodes. This will very likely increase the reliability of the whole module and will lead to much lower failure rates in the field, which is another argument for using these smart BPDs as they improve lifetime of modules and consequently reliability of PV systems.

7. CONCLUSIONS

In this work, we confirm by experiment and simulation that a new generation of BPDs with much lower power dissipation and voltage drops than present day BPDs can be used to increase the shading tolerance of conventional solar modules. Measurements and simulations were performed for a series of different topologies, shadow materials (cardboard and wire mesh), and shadow patterns (row, column, random, and corner). Measurements were validated with a simulation model created in Python, which performed well, especially considering the many different configurations, materials, and shadow patterns that were simulated. The extent of the performance increase is highly dependent on the shape of the shading pattern, its transmission, and the configuration of the BPDs. Once more than ~20 diodes are incorporated in a 60-cell module, the performance of a module stabilizes in the sense that the yield is less affected by shading. For our cardboard experiments, the use of 20 smart BPDs (one BPD per three cells) leads to an improvement of a factor 3 in power output under shading conditions; for

our netting experiments, a factor 1.5 is found. Besides, performance increase as a result of higher shade resilience; also, lower BPD temperatures will lead to increased reliability in the field. Cost of smart BPDs is now hampering widespread use; however, economic feasibility can be expected once these BPDs are produce by the millions. Because of the low voltage drop of the smart BPDs, even one BPD per cell could be incorporated, which is not possible with conventional diodes. Of course, this would increase the module cost without additional shading resilient action.

ACKNOWLEDGEMENTS

REFERENCES

1. IEA PVPS. Trends 2016 in photovoltaic applications, 21th edition, IEA-PVPS T1-30:2016, International Energy Agency, 2016, http://www.iea-pvps.org/index.php?id=256 (last accessed 5 March 2017).

2. SolarPower Europe. Global market outlook for solar power, 2016–2020, 2016. http://www.solarpowereurope.org/fileadmin/user_upload/documents/Events/SolarPower_Webinar_Global_Market_Outlook.pdf (last accessed 5 March 2017).

3. Pennisi S, Pulvirenti F, La Scala A. Low-power cool bypass switch for hot spot prevention in photovoltaic panels. *ETRI Journal* 2011; **33**: 880–886.

4. Kim KA, Krein PT. Reexamination of photovoltaic hot spotting to show inadequacy of the bypass diode. *IEEE Journal of Photovoltaics* 2015; **5**: 1435–1441.

5. Bidram A, Davoudi A, Balog RS. Control and circuit techniques to mitigate partial shading effects in photovoltaic arrays. *IEEE Journal of Photovoltaics* 2012; **2**: 532–546.

6. La Manna D, Vigni VL, Sanseverino ER, Di Dio V, Romano P. Reconfigurable electrical interconnection strategies for photovoltaic arrays: a review. *Renewable and Sustainable Energy Reviews* 2014; **33**: 412–426.

7. Deline C, Meydbray J, Donovan M, Forrest J. Photovoltaic shading testbed for module-level power electronics, *NREL/TP-5200-54876*, NREL, Golden, 2012, http://www.nrel.gov/docs/fy12osti/54876.pdf (last accessed 5 March 2017).

8. Nguyen D, Lehman B. An adaptive solar photovoltaic array using model-based reconfiguration algorithm. *IEEE Transactions on Industrial Electronics* 2008; **55**: 2644–2654.

9. Velasco-Quesada G, Guinjoan-Gispert F, Pique-Lopez R, Roman-Lumbreras M, Conesa-Roca A, Electrical PV. Array reconfiguration strategy for energy extraction improvement in grid-connected PV systems. *IEEE Transactions on Industrial Electronics* 2009; **56**: 4319–4331.

10. Roets J. Optimalisatie van de energie-omzetting in zonnepanelen door actieve cel-reconfiguratie, PhD Thesis, Universiteit Gent, 2012, http://lib.ugent.be/fulltxt/RUG01/001/886/971/RUG01-001886971_2012_0001_AC.pdf (last accessed 5 March 2017).

11. Wang Y, Lin X, Kim Y, Chang N, Pedram M. Architecture and control algorithms for combating partial shading in photovoltaic systems. *IEEE Transactions on Computer-Aided Design of Integrated Circuits and Systems* 2014; **33**: 917–930.

12. Ollala C, Clement D, Rodriquez M, Maksimovic D. Architectures and control of submodule integrated DC-DC converters for photovoltaic applications. *IEEE Transactions on Power Electronics* 2013; **28**: 2980–2997.

13. Bergveld HJ, Büthker D, Castello C, Doorn T, De Jong A, Van Otten R, De Waal K. Module-level DC/DC conversion for photovoltaic systems: the delta-conversion concept. *IEEE Transactions on Power Electronics* 2013; **28**: 2005–2013.

14. Carr A, Jansen MJ, De Bruijne M, Kloos MJH, Eerenstein W. A high voltage MWT module with improved shadow performance, *Proceedings 40th Photovoltaic Specialists Conference*, Denver, 2014, DOI: https://doi.org/10.1109/PVSC.2014.6925482

15. Texas Instruments. SM74611 smart bypass diode, http://www.ti.com/lit/ds/symlink/sm74611.pdf (last accessed 5 March 2017).

16. Green MA, Gauja E, Withayachamnakul W. Silicon solar cells with integral bypass diodes. *Solar Cells* 1981; **3**: 233–244.

17. Hasyim ES, Wenham SR, Green MA. Shadow tolerance of modules incorperating integral bypass diode solar cells. *Solar Cells* 1986; **19**: 109–122.

18. Roche D, Outhred H, Kaye RJ. Analysis and control of mismatch power loss in photovoltaic arrays. *Progress in Photovoltaics: Research and Applications* 1995; **3**: 115–127.

19. Lefevre B, Peeters S, Poortmans J, Driesen J. Predetermined static configurations of a partially shaded photovoltaic module. *Progress in Photovoltaics: Research and Applications* 2017; **25**: 149–160.

20. Reinders A, Verlinden P, Van Sark W, Freundlich A. *Photovoltaic Solar Energy: From Fundamental to Applications*. Wiley: New York, 2017.

21. Bishop JW. Computer simulation of the effects of electrical mismatches in photovoltaic cell interconnection circuits. *Solar cells* 1988; **25**: 73–89.

22. Woyte A, Nijs J, Belmans R. Partial shadowing of photovoltaic arrays with different system configurations: literature review and field test results. *Solar Energy* 2003; **74**: 217–233.

23. Sinapis K, Tzikas C, Litjens G, Van den Donker M, Folkerts W, Van Sark W. A comprehensive study on partial shading response of c-Si modules and yield modeling of string inverter and module level power electronics. *Solar Energy* 2016; **135**: 731–741.

24. Reich NH, Mueller B, Armbruster A, Van Sark WGJHM, Performance ratio revisited: is PR > 90% realistic?, *Progress in Photovoltaics: Research and Applications*, 2012; **20**: 717–726.

25. Fertig F, Rein S, Schubert M, Warta W. Impact of junction breakdown in muti-crystalline silicon solar cells on hot spot formation and module performance, *Proceedings of the 26th European PV Solar Energy Conference and Exhibition*, Hamburg, 2011; 1168–1178.

26. Kurtz S. Photovoltaic module reliability workshop 2013, *NREL/TP-5200-60167*, NREL, Golden, 2013, http://www.nrel.gov/docs/fy14osti/60167.pdf (last accessed 5 March 2017).

27. Köntges M, Kurtz S, Packard C, Jahn U, Berger KA, Kato K, Friesen T, Liu H, Van Iseghem M. Review of failures of photovoltaic modules, *IEA-PVPS T13–01:2014*, International Energy Agency, 2014, http://iea-pvps.org/index.php?id=275 (last accessed 5 March 2017).

28. Kurokawa K. Realistic values of various parameters for PV system design. *Renewable Energy* 1988; **15**: 157–164.

29. Erge T, Hoffmann VU, Kiefer K, Rössler E, Rindelhardt U, Teichmann T, Decker B, Grochowski J, Heilscher G, Schneider M, Blässer G, Ossenbrink H, Becker H, Vaaßen W, GEnnening B, Rieß H, Sprau P, The German 1000-Roofs-PV-programme—a resume of the 5 years pioneer project for small grid-connected PV systems, *Proceedings 2nd World Conference on Photovoltaic Solar Energy Conversion*, Vienna, 1998; 2648–2651.

30. Ueda Y, Kurokawa K, Kitamura K, Yokota M, Akanuma K, Sugihara H. Performance analysis of various system configurations on grid-connected residential PV systems. *Solar Energy Materials and Solar Cells* 2009; **93**: 945–949.

31. Leloux J, Narvarte L, Trebosc D. Performance analysis of 10,000 residential PV systems in France and

Belgium, *Proceedings of the 26th European Photovoltaic Solar Energy Conference*, Hamburg, 2011; 3939–3946.

32. Van Sark WGJHM, 't Hart S, De Jong MM, De Rijk P, Moraitis P, Kausika BB, Van der Velde H. "Counting the sun"—a Dutch public awareness campaign on PV performance, *Proceedings of the 29th European Photovoltaic Solar Energy Conference*, Amsterdam, 2014; 4161–4164.

33. Deline C. Partially shaded operation of a grid-tied PV system, *Proceedings 34th IEEE Photovoltaic Specialists Conference*, Philadelphia, 2009; 1268–1273.

34. Pennington B, Gupta S, Saxton P, Eden D, Green L, Fleshman J. Guidelines for California's solar electric incentive programs (senate bill 1) second edition, CEC-300-2008-007-CMF, 2008. http://www.energy.ca.gov/2008publications/CEC-300-2008-007/CEC-300-2008-007-CMF.PDF (last accessed 5 March 2017).

35. Silvestre S, Boronat A, Chouder A. Study of bypass diodes configuration on PV modules. *Applied Energy* 2009; **86**: 1632–1640.

36. Alonso-Garcia MC, Ruiz JM, Chenlo F. Experimental study of mismatch and shading effects in the I–V

characteristics of a photovoltaic module. *Solar Energy Materials and Solar Cells* 2006; **90**: 329–340.

37. Van Sark WGJHM, Louwen A, De Waal AC, Schropp REI. UPOT: the Utrecht photovoltaic outdoor test facility, *Proceedings of the 27th European Photovoltaic Solar Energy Conference*, Frankfurt, 2012; 3247–3249.

38. Stein JS. The photovoltaic performance modeling collaborative (PVPMC), *Proceedings 38th Photovoltaic Specialists Conference*, Austin, 2012; 3048–3052.

39. Jain A, Kapoor A. Exact analytical solutions of the parameters of real solar cells using Lambert W-function. *Solar Energy Materials and Solar Cells* 2004; **81**: 269–277.

40. De Soto W, Klein SA, Beckman WA. Improvement and validation of a model for photovoltaic array performance. *Solar Energy* 2006; **80**: 78–88.

41. Lim J-R, Min YK, Jung T-H, Ahn J-H, Ahn H-K. Correlation between reverse voltage characteristics and bypass diode operation with different shading conditions for c-Si photovoltaic module package. *Journal of Semiconductor Technology and Science* 2015; **15**: 577–583.